

THE FIRST GLITCH IN A CENTRAL COMPACT OBJECT PULSAR: 1E 1207.4–5209

E. V. GOTTHELF AND J. P. HALPERN

Columbia Astrophysics Laboratory, Columbia University, New York, NY 10027-6601, USA; eric@astro.columbia.edu

ABSTRACT

Since its discovery as a pulsar in 2000, the central compact object (CCO) 1E 1207.4–5209 in the supernova remnant PKS 1209–51/52 had been a stable 0.424 s rotator with an extremely small spin-down rate and weak ($B_s \approx 9 \times 10^{10}$ G) surface dipole magnetic field. In 2016 we observed a glitch from 1E 1207.4–5209 of at least $\Delta f/f = (2.8 \pm 0.4) \times 10^{-9}$, which is typical in size for the general pulsar population. However, glitch activity is closely correlated with spin-down rate \dot{f} , and pulsars with \dot{f} as small as that of 1E 1207.4–5209 are never seen to glitch. Unlike in glitches of ordinary pulsars, there may have been a large increase in \dot{f} as well. The thermal X-ray spectrum of 1E 1207.4–5209, with its unique cyclotron absorption lines that measure the surface magnetic field strength, did not show any measurable change after the glitch, which rules out a major disruption in the dipole field as a cause or result of the glitch. A leading theory of the origin and evolution of CCOs, involving prompt burial of the magnetic field by fall-back of supernova ejecta, might hold the explanation for the glitch.

Subject headings: ISM: individual (PKS 1209–51/52) — pulsars: individual (1E 1207.4–5209, PSR J1210–5226) — stars: neutron

1. INTRODUCTION

The group of ≈ 10 central compact objects (CCOs) in supernova remnants (SNRs) are defined by their steady surface thermal X-ray emission, lack of surrounding pulsar wind nebula, and non-detection at any other wavelength. Of the eight well-established CCOs, three were found to be pulsars (Zavlin et al. 2000; Gotthelf et al. 2005, 2009). Their spin-down properties provide an estimate of surface dipole magnetic field strength via $B_s = 3.2 \times 10^{19} \sqrt{\dot{f}/f^3}$ of $(2.8, 3.1, 9.8) \times 10^{10}$ G (Halpern & Gotthelf 2010; Gotthelf et al. 2013a), two orders of magnitude less than those of canonical young pulsars. The homogeneous X-ray properties of the remaining CCOs that have not yet been seen to pulse suggest that they have similar or even weaker magnetic fields than the known CCO pulsars, or a more uniform surface temperature, or a more aligned geometry. The fact that CCOs are found in SNRs in comparable numbers to other classes of young neutron stars (NSs) implies that they must represent a significant fraction of NS births.

1E 1207.4–5209 in the SNR PKS 1209–51/52 is the first CCO pulsar discovered (Zavlin et al. 2000) and the most intensively studied. It is also the first isolated NS to display strong absorption lines in its X-ray spectrum (Sanwal et al. 2002; Mereghetti et al. 2002; Bignami et al. 2003; De Luca et al. 2004). The evenly spaced spectral features are widely accepted as the electron cyclotron fundamental at $E_0 = 0.7$ keV and its harmonics in a magnetic field of $B \approx 8 \times 10^{10}$ G. [More precisely, these features are due to quantum oscillations in the free-free opacity (Suleimanov et al. 2010)]. This is the first measurement of the surface magnetic field on a CCO by a direct technique that is independent of timing, and the result is fully consistent with the magnetic field inferred from its spin-down, $B_s = 9.8 \times 10^{10}$ G.

In a series of papers (Gotthelf et al. 2007; Halpern & Gotthelf 2011; Gotthelf et al. 2013a; Halpern & Gotthelf 2015) we have followed the long-term timing properties of 1E 1207.4–5209 which, until 2014, showed steady

spindown with no evidence of timing noise or glitches. Glitches are sudden increases in spin frequency that are thought to result from either “starquakes,” stress relief of the NS crust (e.g., Link et al. 1998), or the sudden unpinning and repinning of neutron superfluid vortices in the inner crust (Alpar et al. 1984). Glitch activity among pulsars is correlated mainly with frequency derivative, such that pulsars with $|\dot{f}|$ as small as those of CCOs have never been seen to glitch (Espinoza et al. 2011; Fuentes et al. 2018). Nevertheless, interior properties of CCOs may be similar to those of canonical young pulsars, which may cause them to glitch (Ho 2015).

We present new observations of 1E 1207.4–5209 in 2016–2018 that detect a glitch for the first time in a CCO. In Section 2, we describe the new X-ray timing observations. Section 3 details the timing properties of the detected glitch, while Section 4 compares the pre- and post-glitch spectrum and flux to search for any changes. In Section 5, we compare the properties of this glitch to the ensemble of measured NS glitches, and discuss its implications for theories of the internal structure and evolution of CCOs. An alternative model of accretion-torque fluctuations is also briefly considered. Conclusions and suggestions for follow-up work are described in Section 6.

2. NEW X-RAY OBSERVATIONS

In the course of monitoring of 1E 1207.4–5209 we found that the phase of the pulsar measured in 2016 July no longer followed the prediction of the prior ephemeris. We obtained a new set of *XMM-Newton* observations to confirm the glitch and characterize its properties. Six observations in 2017 June–December were used to bootstrap a new timing solution. Then we began semi-annual *XMM-Newton* observations in 2017 and 2018 that supplement our annual *Chandra* monitoring. A log of the observations obtained since 2016 is presented in Table 1. Here we describe these data sets.

We concentrate on *XMM-Newton* data obtained with the European Photon Imaging Camera (EPIC) pn and MOS detectors. Data from the Reflection Grating Spec-

TABLE 1
LOG OF NEW X-RAY TIMING OBSERVATIONS OF 1E 1207.4–5209

Mission	Instrument /Mode	ObsID	Date (UT)	Exposure (ks)
<i>XMM</i>	EPIC-pn/SW	0780000201	2016 Jul 28	34.0
<i>XMM</i>	EPIC-pn/SW	0800960201	2017 Jun 22	34.8
<i>XMM</i>	EPIC-pn/SW	0800960301	2017 Jun 23	22.2
<i>XMM</i>	EPIC-pn/SW	0800960401	2017 Jun 24	24.1
<i>XMM</i>	EPIC-pn/SW	0800960501	2017 Jul 03	25.0
<i>XMM</i>	EPIC-pn/SW	0800960601	2017 Aug 10	21.3
<i>Chandra</i>	ACIS-S3/CC	19612	2017 Oct 10	33.0
<i>XMM</i>	EPIC-pn/SW	0800960701	2017 Dec 24	21.3
<i>XMM</i>	EPIC-pn/SW	0821940201	2018 Jun 22	33.4
<i>Chandra</i>	ACIS-S3/CC	19613	2018 Aug 27	66.6

trometers are not used in this work. The EPIC pn (Strüder et al. 2001) sits at the focal plane of a coaligned, multi-nested foil mirror with an on-axis point spread function with FWHM of $\approx 12''.5$ at 1.5 keV. The EPIC instruments are sensitive to X-rays in the 0.15–12 keV range with moderate energy resolution of $E/\Delta E(\text{pn}) \sim 20\text{--}50$. In order to resolve the 0.424 s pulse of 1E 1207.4–5209, the EPIC pn data were obtained in *PrimeSmallWindow* mode ($4'.3 \times 4'.3$), which has high time resolution of 6 ms at the expense of 29% deadtime. Data acquired with the two MOS detectors (Turner et al. 2001) were obtained in *PrimePartialW2* small-window mode on the central CCD with a $1'.8 \times 1'.8$ FoV. The time resolution in this mode is 0.3 s, insufficient to resolve the pulsations of 1E 1207.4–5209. The MOS cameras, less sensitive at the lower energy range of 1E 1207.4–5209, were used only to confirm the EPIC pn spectral results.

The *XMM-Newton* data were reduced and analyzed using the Standard Analysis Software (SAS) version 15.0.0 with the most up-to-date calibration files. After filtering out background flares we obtained usable exposure times listed in Table 1. For the timing analysis all photon arrival times were converted to barycentric dynamical time (TDB) using the DE405 solar system ephemeris and the *Chandra* coordinates in Gotthelf et al. (2013a).

We also examined the *Chandra* observations that fell within the post-glitch time interval (see Table 1). The pulsar was placed on the S3 CCD of the Advanced Camera for Imaging and Spectroscopy (ACIS), which was run in continuous-clocking mode that provides a time resolution of 2.85 ms. We processed this data set following the method outlined in Gotthelf et al. (2007) and Halpern & Gotthelf (2011).

3. TIMING ANALYSIS

Prior to 2015, a unique, quadratic ephemeris from *XMM-Newton* and *Chandra* observations of 1E 1207.4–5209 adequately described its rotation for 14 years (Halpern & Gotthelf 2015). Then, on 2016 July 28, we found a large ($\Delta\phi \approx -0.35$) and significant (18σ) deviation in phase between the observed pulse arrival time and that predicted from the pre-2015 ephemeris, consistent with the pulse arriving earlier than expected. Using the subsequent observations, we generated additional pulse times-of-arrival (TOAs) following the recipe given in our previous papers (Halpern & Gotthelf 2011; Gotthelf et al. 2013a) and continued to compare them to the pre-2015 ephemeris. The persistent deviation in

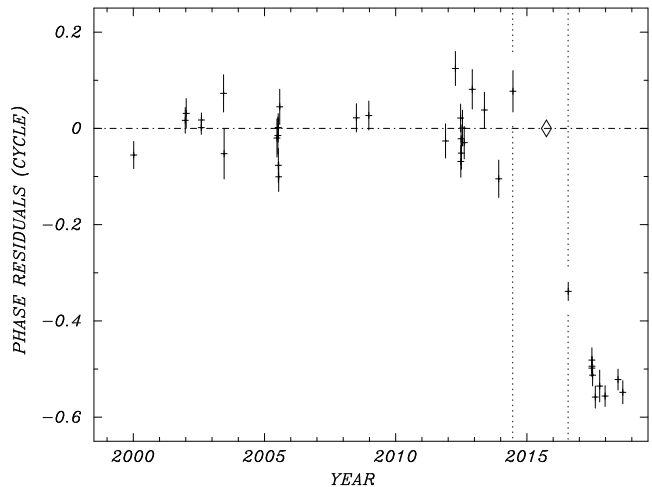


FIG. 1.— Pulse-phase residuals from the timing solution of Halpern & Gotthelf (2015), with the addition of the ten post-2015 *XMM-Newton* data points. A glitch occurred some time during the interval denoted by the vertical dotted lines. By matching the phase of the pre- and post-glitch ephemerides, the estimated glitch time indicated by the diamond is 2015 September 30.

phase over time is clearly evident in Figure 1 as a highly significant shift of up to ≈ -0.55 cycles from the pre-2015 ephemeris. This is standard behavior for a glitch, namely, a speed-up in the spin frequency f causes the pulses to come successively earlier than the pre-glitch ephemeris predicts.

We also checked for any change in pulse shape and pulsed fraction, in case what we think is a glitch might be due instead to a change in the location of a hot spot on the surface, or the emergence of a new emission process. There is no significant difference between pre- and post-glitch pulse shape, pulsed fraction, or energy dependence of pulse phase, indicating that the surface thermal emission pattern has not changed. So a simple glitch is the most straightforward interpretation of Figure 1.

Because of the long, 2-year gap in observations between 2014 and 2016, we cannot be certain of the exact residual cycle count after the glitch, nor determine the epoch of the glitch with any precision. Fitting possible linear slopes to a few points after the glitch in Figure 1 implies that the glitch magnitude is $\Delta f/f = (2.8 \pm 0.4) \times 10^{-9}$, which is the minimum possible magnitude corresponding to the minimum possible phase shift, as plotted. We also have independent evidence for an increase in frequency by fitting a new, phase-connected quadratic ephemeris to the ten post-glitch points from 2016 July 28 to 2018 Aug 27. In this fit, $\Delta f/f_{\text{pred}} = (5.22 \pm 0.80) \times 10^{-9}$ (at a glitch epoch of MJD 57295 = 2015 September 30), which is not precise enough to confirm the phase counting in Figure 1, but does suggest a larger glitch magnitude than the simple linear fit. Both pre- and post-glitch ephemerides are listed in Table 2.

Post-glitch behavior typically includes partial recovery toward the pre-glitch ephemeris, which can be fitted as a glitch also in \dot{f} that subsequently decays on one or more time scales (see examples in Espinoza et al. 2011). In this context, our post-glitch ephemeris only crudely estimates an average value for the post-glitch f because the data points are not precise or numerous enough to

TABLE 2
 EPHEMERIDES FOR 1E 1207.4–5209

Parameter	Value ^a
R.A. (J2000)	12 ^h 10 ^m 00 ^s .91
Decl. (J2000)	−52°26′28″.4
Surface dipole field, B_s	9.8×10^{10} G
Spin-down luminosity, \dot{E}	1.2×10^{31} erg s ^{−1}
Characteristic age, $\tau_c \equiv P/2\dot{P}$	301 Myr
Pre-glitch Timing Solution (2000–2014)	
Epoch of ephemeris (MJD TDB)	53562.00000052
Span of ephemeris (MJD)	51549–56829
Frequency, f	2.357763502866(65) s ^{−1}
Frequency derivative, \dot{f}	$-1.2398(83) \times 10^{-16}$ s ^{−2}
Period, P	0.424130748815(12) s
Period derivative, \dot{P}	$2.230(14) \times 10^{-17}$
χ^2_{ν} (DoF)	2.68(25)
Post-glitch Timing Solution (2016–2018)	
Epoch of ephemeris (MJD TDB)	57977.0000040
Span of ephemeris (MJD)	57597–58358
Frequency, f	2.35776345859(38) s ^{−1}
Frequency derivative, \dot{f}	$-2.82(31) \times 10^{-16}$ s ^{−2}
Period, P	0.424130756780(68) s
Period derivative, \dot{P}	$5.06(56) \times 10^{-17}$
χ^2_{ν} (DoF)	0.86(7)
Glitch Parameters	
Epoch (MJD)	57295 ^b
Δf	$(1.23 \pm 0.19) \times 10^{-8}$ s ^{−1}
$\Delta f/f_{\text{pred}}$	$(5.22 \pm 0.80) \times 10^{-9}$
$\Delta \dot{f}$	$(-1.58 \pm 0.31) \times 10^{-16}$ s ^{−2}
$\Delta \dot{f}/\dot{f}_{\text{pred}}$	1.27 ± 0.25

^aUncertainties in the last digits are given in parentheses.

^bEpoch for the glitch estimated by matching the zero phase of the two timing solutions; this assumes a constant post-glitch \dot{f} .

track any change in \dot{f} . Nevertheless, a post-glitch \dot{f} is significantly detected at $(-2.82 \pm 0.31) \times 10^{-16}$ s^{−2}, which is larger than the historical value of $(-1.2398 \pm 0.0083) \times 10^{-16}$ s^{−2}.

4. SPECTRAL ANALYSIS

We also examined the pre- and post-glitch *XMM-Newton* spectra of 1E 1207.4–5209 to look for any change by comparing six observations obtained in 2012 and six in 2017. For each EPIC pn observation we extracted spectra using an aperture of radius 0′.5 and a nearby off-source circular region of radius 1′.0. Response matrices and effective area files were generated for each observation using the SAS software suite. We combined the spectra extracted from the pre- and post-glitch observations, respectively, using the FTOOL *addascapec* to produce a single source spectrum and associated files at each epoch. These spectra were grouped to include at least 200 counts per channel and were fitted using XSPEC v12.10.0c software (Arnaud 1996). The two spectra were fitted simultaneously to a two-blackbody model with interstellar absorption and cyclotron lines in the range 0.3–2.5 keV. We characterize the column density using the TBabs absorption model, selecting the *wilm* Solar abundances (Wilms et al. 2000) and the *vern* photoionization cross-section (Verner et al. 1996).

We note that it is not possible to uniquely fit the

 TABLE 3
 1E 1207.4–5209 *XMM-Newton* SPECTRAL FITTING

Parameter	Pre-glitch ^a	Post-glitch ^b
Epoch	2012	2017
N_{H} (cm ^{−2}) (fixed)	1.66×10^{21}	1.66×10^{21}
kT_1 (keV)	$0.0801^{+0.0046}_{-0.0042}$	$0.0742^{+0.0042}_{-0.0037}$
kT_2 (keV)	$0.2513^{+0.0022}_{-0.0021}$	$0.2509^{+0.0021}_{-0.0021}$
E_0 (keV)	$0.712^{+0.012}_{-0.011}$	$0.710^{+0.017}_{-0.015}$
σ_0 (keV) (fixed)	0.08	0.08
τ_0	0.26	0.22
E_1 (keV)	$1.4292^{+0.0087}_{-0.0088}$	$1.4216^{+0.0089}_{-0.0090}$
σ_1 (keV) (fixed)	0.08	0.08
τ_1	0.098	0.10
F_x (pn) ^c	$2.084^{+0.010}_{-0.011}$	$2.078^{+0.010}_{-0.012}$
χ^2_{ν} (DoF)	1.39(283)	1.32(276)

Notes — EPIC pn spectral fit in the 0.3–2.5 keV range, with the column density and Gaussian line widths held fixed (see text). Uncertainties on kT and E are given at the 68% confidence level for 4 interesting parameters. Uncertainty on the flux is given at the 90% confidence level.

^aPre-glitch live time 107 ks from ObsIDs 0679590101/201/301/401/501/601.

^bPost-glitch live time 98 ks from ObsIDs 0800960201/301/401/501/601/701.

^cAbsorbed 0.3–2.5 keV flux in units of 10^{-12} erg cm^{−2} s^{−1}.

column density, softer blackbody kT_1 , and the absorption features simultaneously. Furthermore, the detailed shape of the absorption features is not known. We used a Gaussian line whose width is fixed to the minimum value needed to characterize the absorption and then fixed the column density to the average overall value for this fixed Gaussian width. We consider this a representative model in order to effectively compare the pre- and post-glitch spectrum.

The results of the fits are presented in Table 3. The residuals from the pre-glitch two-blackbody model are shown in Figure 2 to highlight any differences. The prominent absorption features are consistent with an electron cyclotron fundamental ($E_0 = 0.7$ keV) and its harmonics in magnetic field of $B \approx 8 \times 10^{10}$ G, according to the relation $E_0 = 1.16 (B/10^{11} \text{ G})/(1+z)$ keV, where $z \approx 0.3$ is the gravitational redshift. Within the statistics of the spectra, we find no change in the spectrum from 2012 to 2017, specifically, no definite shift in E_0 that would indicate a change in surface magnetic field strength after the glitch. Instead, the field strength is seen to be constant to $\approx 2\%$. The two temperatures and total flux are also unchanged, the latter at the 0.5% level.

5. DISCUSSION

5.1. Glitch Magnitude

The distribution of glitch magnitudes in pulsars is bimodal, with a broad peak centered at $\Delta f/f \approx 3 \times 10^{-9}$, and a narrow peak at $\Delta f/f \approx 1 \times 10^{-6}$ (Espinoza et al. 2011). The glitch in 1E 1207.4–5209 is thus typical of the lower-amplitude group, and also of glitch sizes in the Crab pulsar. However, it is unprecedented for a pulsar with the timing properties of 1E 1207.4–5209 to even have a glitch. Glitch activity correlates best with the

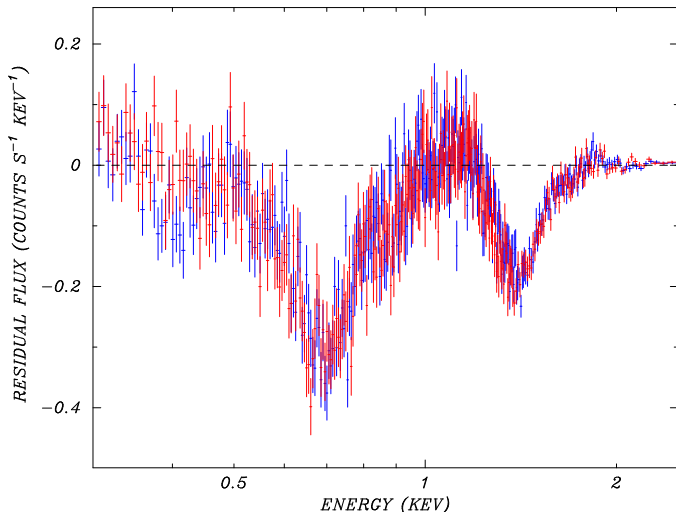


FIG. 2.— Comparison of the pre- and post-glitch spectra of 1E 1207.4–5209 using combined *XMM-Newton* EPIC pn data acquired in 2012 (blue) and in 2017 (red). Residuals from the best fit pre-glitch two-temperature blackbody model given in Table 3 with the absorption lines removed are compared to the post-glitch spectrum using the same model parameters. Electron cyclotron features at 0.7 keV and 1.4 keV are evident, but there is no significant change in the line centroids, and thus the magnetic field strength, following the glitch.

spin-down rate of pulsars in a linear manner such that the average amount of spin-down reversed in a glitch, \dot{f}_g , is $\approx 0.01|\dot{f}|$, i.e., 1% of the long-term spin-down is reversed (Espinoza et al. 2011; Fuentes et al. 2018). This has been interpreted in terms of the the vortex creep theory (Alpar et al. 1984) to imply that 1% or more of the moment of inertia of the NS is contained in a crustal superfluid whose vortices are repeatedly pinned and unpinned.

In this picture, it is natural that pulsars with small \dot{f} would not glitch frequently. Among pulsars with $|\dot{f}| < 1 \times 10^{-15} \text{ s}^{-2}$, only three glitches have been observed in ≈ 4260 pulsar-years of monitoring, and no pulsar with $|\dot{f}| < 3 \times 10^{-16} \text{ s}^{-2}$ has glitched in 1780 yr (Fuentes et al. 2018). For 1E 1207.4–5209 with its $\dot{f} = -1.24 \times 10^{-16} \text{ s}^{-2}$ to have glitched once in 15 years of monitoring makes it, therefore, a significant outlier with 99% confidence.

In addition, typical glitches in $\Delta\dot{f}/\dot{f}$ are only $\sim 10^{-3} - 10^{-2}$, much smaller than the order unity change in 1E 1207.4–5209 if we take its post-glitch ephemeris literally. In magnetars, however, it is common to see glitches in \dot{f} of order unity (Kaspi et al. 2003; Dib et al. 2008; Dib & Kaspi 2014), but these could be due to magnetospheric phenomena such as particle winds and rearrangement of twisted magnetic field lines that change the dipole moment by a large factor. In CCOs there is no magnetospheric activity and, uniquely testable in the case of 1E 1207.4–5209, no change in the surface dipole magnetic field strength from the energies of the cyclotron lines. Therefore, it is more likely that the change in \dot{f} , if real, is due to internal torques between the superfluid and normal matter. However, $\Delta\dot{f}/\dot{f}$ is too large to be explained by vortex pinning unless most of the moment of inertia of the NS can become pinned.

There is a class of intermittent radio pulsars, whose $|\dot{f}|$ is larger by a factor of order unity when they are turned on as radio pulsars in comparison with their off states (e.g., Lyne et al. 2017). States can persist for days up to years, with the most extreme example being that of PSR J1841–0500 (Camilo et al. 2012), which was off for 540 days. Its $|\dot{f}|$ was higher by a factor of 2.5 while the radio pulsations were turned on. The implication is that a magnetospheric plasma is present and contributing to the spin-down torque only during the radio on state. If the glitch triggered a transition to a magnetospheric active state in 1E 1207.4–5209, then its higher $|\dot{f}|$ could be an indicator that it has turned on as a radio pulsar. We reserve judgment on this unexpected result until future observations can measure a new, long-term value of \dot{f} with a precision comparable to the pre-glitch ephemeris.

5.2. CCO Structure and Evolution

Although the glitch activity of 1E 1207.4–5209 would not have been predicted from its small \dot{f} and weak surface dipole field B_s , its internal magnetic field may be as strong as those of canonical young pulsars that do glitch, according to two arguments. First, the thermal X-ray pulsations by which CCO pulsars are discovered are difficult to explain in the context of weak magnetic fields, since the only mechanism thought to be capable of creating a non-uniform surface temperature is anisotropic heat conduction in a strong magnetic field. The effects of different magnetic field configurations on heat transport in the crust and envelope of NSs were modeled by Geppert et al. (2004), Geppert et al. (2006), Pérez-Azorín et al. (2006), and Pons et al. (2009). A toroidal field is expected to be the initial configuration generated by differential rotation in the proto-NS dynamo (Thompson & Duncan 1993). One of the effects of crustal toroidal field is to insulate the magnetic equator from heat conduction, resulting in warm spots at the poles. To have a significant effect on heat transport, the crustal toroidal field strength required in all models is $> 10^{14} \text{ G}$, many orders of magnitude greater than the poloidal field if the latter is measured by the spin-down. Shabaltas & Lai (2012) tried to model the pulse profile of the CCO PSR J1852+0040 in Kes 79 with anisotropic conduction in such a model, and concluded that they needed a toroidal crustal field of $B_\phi > 2 \times 10^{14} \text{ G}$ to achieve the large observed pulsed fraction of $64 \pm 2\%$, although they could not actually match the broad pulse shape (see also Bogdanov 2014a.)

Second, a theory of CCOs posits that they are born with a canonical NS magnetic field that was buried by fall-back of a small amount of supernova ejecta, $\sim 10^{-4} M_\odot$, during the hours and days after the explosion. The buried field will diffuse back to the surface on a timescale of $\sim 10^5 \text{ yr}$ (Geppert et al. 1999; Bernal et al. 2010, 2013; Ho 2011, 2015; Viganò & Pons 2012). During this time the CCO will move vertically up in the $P - \dot{P}$ diagram due to its rapidly increased braking as the dipole field grows (see Figure 1 of Luo et al. 2015). Eventually it will join the bulk of the population of ordinary radio pulsars. Such a scenario addresses the absence of CCO descendants that should remain in the same region of $P - \dot{P}$ space long after their natal SNRs fade, if their weak magnetic fields are intrinsic. Searches for a thermal X-ray signature from such CCO descendants have

yet to find a single example (Gotthelf et al. 2013b; Bogdanov et al. 2014b; Luo et al. 2015), except *possibly* for the unusual X-ray pulsar Calvera (Halpern et al. 2013; Halpern & Gotthelf 2015). The field growth hypothesis also has the feature of not requiring yet another class of NS to exist that would only exacerbate the apparent excess of pulsars with respect to the Galactic core-collapse supernova rate (Keane & Kramer 2008).

More generally, magnetic field growth (Blandford et al. 1983) or dipole axis counteralignment (Macy 1974) have long been considered possible reasons why most measured pulsar braking indices, defined as $n \equiv f\dot{f}/\dot{f}^2$, are less than the static dipole value of 3. If the dipole magnetic field strength B_s is increasing at the rate \dot{B}_s , the braking index is reduced to

$$n = 3 - 2 \frac{\dot{B}_s f}{B_s |\dot{f}|}.$$

Ho (2015) calculated that the upward vectors in the $P-\dot{P}$ diagram of three pulsars with $n < 1.7$, namely, PSR B0833–45 (Vela), PSR J0537–6910 in the LMC, and PSR J1734–3333, could be explained by the same processes of field burial and diffusion as in CCOs, but with a smaller amount of accreted mass, $\sim 10^{-5} M_\odot$. These three pulsars also happen to have large glitches, in the upper peak of the bimodal distribution of glitch magnitudes. The possible connection of low braking index to regular, large glitches, led Ho (2015) to propose that this type of glitch activity could be triggered by the motion of magnetic fields through the NS crust, interacting with the neutron superfluid there. Although only a small glitch has been seen from 1E 1207.4–5209, it is interesting to consider that, even though there is no evidence that glitch activity is correlated with *dipolar* magnetic field strength (Fuentes et al. 2018), a glitch may be triggered by motion of *internal* magnetic field.

5.3. Accretion Torque Noise?

Here we consider an alternative interpretation of the apparent glitch: torque noise during low-level accretion, possibly from a fall-back debris disk, following the arguments in Halpern et al. (2007). While the B -field of 1E 1207.4–5209 derived from timing only assumes dipole braking, its spin parameters fall in a regime where both dipole braking and accretion disk torques are conceivably significant. Accretion at a rate $\dot{M} = 10^{11} \text{ g s}^{-1}$ (or less if the NS magnetic field is weaker) can penetrate the light cylinder to the magnetospheric radius. If so, the system is in the propeller regime, in which matter flung out takes angular momentum from the NS, causing it to spin down. The propeller spin-down rate is

$$\dot{f} \approx -9.5 \times 10^{-15} \mu_{29}^{8/7} \dot{M}_{13}^{3/7} \left(\frac{M_{\text{NS}}}{M_\odot} \right)^{-2/7} \\ \times I_{45}^{-1} \left(\frac{f}{2.357 \text{ Hz}} \right) \left(1 - \frac{f_{\text{eq}}}{f} \right) \text{ s}^{-2}$$

(Menou et al. 1999). Here I_{45} is the NS moment of inertia in units of 10^{45} g cm^2 , $\mu_{29} = B_s R_{\text{NS}}^3$ is the magnetic dipole moment in units of 10^{29} G cm^3 , \dot{M}_{13} is the mass transfer rate in units of 10^{13} g s^{-1} , and f_{eq} is the equilibrium spin frequency, presumed to be $\ll f$ because of

the young age and small \dot{M} . In this model \dot{M} is the rate of mass expelled, which must be $> \dot{m}$, the accretion rate onto the NS. While \dot{m} must be $< 3 \times 10^{13} \text{ g s}^{-1}$ so as not to exceed the bolometric luminosity of 1E 1207.4–5209, $\approx 2.5 \times 10^{33} \text{ erg s}^{-1}$, even such a small accretion rate is ruled out by upper limits on accretion-disk luminosity from the non-detection of an optical counterpart by *HST* (De Luca et al. 2011). The latter observation requires an even smaller $\dot{M} < 10^{12} \text{ g s}^{-1}$.

Assuming that $\dot{M} \approx 10^{11} \text{ g s}^{-1}$, accretion contributes negligibly to the luminosity, thus not violating the upper limits on X-ray variability, while still allowing $\dot{f} \approx -1.3 \times 10^{-15} \text{ s}^{-2}$ from the propeller effect. This is a factor of ≈ 4 greater than the \dot{f} of the post-glitch ephemeris. Therefore, fluctuations in the propeller \dot{f} cannot be immediately ruled out as an explanation for the observed timing irregularity. Evolutionary models of fall-back disks predict that an initial disk mass of $< 10^{-6} M_\odot$ can easily supply, at the estimated 7000 yr present age of PKS 1209–51/52, accretion at the above assumed rate (De Luca et al. 2011).

Whether the NS can acquire such a disk from the homologously expanding ejecta moving with it, or from reverse-shocked SN ejecta, depends on details of the explosion. However, if $\sim 10^{-4} M_\odot$ of debris can fall directly onto the NS to bury its magnetic field, it is likely that $10^{-6} M_\odot$ can end up in a disk because of its angular momentum. Not so obvious is the spectrum of timing noise produced at such a low accretion rate, a regime which has thus far not been observed. For now, the overall resemblance of the timing residuals to a classic glitch profile in an isolated pulsar leads us to prefer the glitch model over accretion torque noise.

6. CONCLUSIONS AND FUTURE WORK

We have detected the first glitch in a CCO pulsar, 1E 1207.4–5209. Its frequency jump is at least $\Delta f/f = (2.8 \pm 0.4) \times 10^{-9}$, and possibly larger if a fitted change in \dot{f} by a factor of 2.3 is real. It is crucial to continue timing the pulsar to establish the post-glitch \dot{f} more accurately. A radio pulsation search should be made to test for new magnetospheric activity. There is no evidence for a change in the weak surface magnetic field from the X-ray cyclotron features, and no change in luminosity. Old pulsars with \dot{f} as small as that of 1E 1207.4–5209 have not been seen to glitch, which implies that the glitch mechanism is contingent upon an internal property of this young pulsar, such as high magnetic field strength or temperature. Ho (2015) suggested that diffusion of a previously buried B -field could be the trigger for a glitch. Ho (2015) further suggested that glitches could identify the missing descendants of CCOs. Finding descendants among the ordinary radio pulsar population would solve a major observational problem in CCO evolution, and provide strong support to the field-burial theory of their origin.

This investigation is based on observations obtained with *XMM-Newton*, an ESA science mission with instruments and contributions directly funded by ESA Member States and NASA. Support for this work was provided by NASA through *XMM* grants NNX17AC12G

and 80NSSC18K0452, and *Chandra* Award SAO GO7-18063X issued by the *Chandra* X-ray Observatory Center, which is operated by the Smithsonian Astrophysical

Observatory for and on behalf of NASA under contract NAS8-03060.

REFERENCES

- Alpar, M. A., Pines, D., Anderson, P. W., & Shaham, J. 1984, *ApJ*, 276, 325
- Arnaud, K. A. 1996, in ASP Conf. Ser. 101, *Astronomical Data Analysis Software and Systems V*, ed. G. H. Jacoby & J. Barnes (San Francisco, CA: ASP), 17
- Bernal, C. G., Lee, W. H., & Page D. 2010, *RMxAA*, 46, 309
- Bernal, C. G., Page, D., & Lee, W. H. 2013, *ApJ*, 770, 106
- Bignami, G. F., Caraveo, P. A., De Luca, A., & Mereghetti, S. 2003, *Nature*, 423, 725
- Blandford, R. D., Applegate, J. H., & Hernquist, L. 1983, *MNRAS*, 204, 1025
- Bogdanov, S. 2014, *ApJ*, 790, 94
- Bogdanov, S., Ng, C.-Y., & Kaspi, V. 2014, *ApJ*, 792, L36
- Camilo, F., Ransom, S. M., Chatterjee, S., Johnston, S., & Demorest, P. 2012, *ApJ*, 746, 63
- De Luca, A., Mereghetti, S., Caraveo, P. A., et al. 2004, *A&A*, 418, 625
- De Luca, A., Mignani, R. P., Sartori, A., et al. 2011, *A&A*, 525, 106
- Dib, R., & Kaspi, V. M. 2014, *ApJ*, 784, 37
- Dib, R., Kaspi, V. M., & Gavriil, F. P. 2008, *ApJ*, 673, 1044
- Espinoza, C. M., Lyne, A. G. Stappers, B. W., & Kramer, M. 2011, *MNRAS*, 414, 1679
- Fuentes, J. R., Espinoza, C. M., Reisenegger, A. et al. 2018, *A&A*, 600, A131
- Geppert, U., Küker, M., & Page, D. 2004, *A&A*, 426, 267
- Geppert, U., Küker, M., & Page, D. 2006, *A&A*, 457, 937
- Geppert, U., Page, D., & Zannias, T. 1999, *A&A*, 345, 847
- Gotthelf, E. V., & Halpern, J. P. 2007, *ApJL*, 664, L35
- Gotthelf, E. V., & Halpern, J. P. 2009, *ApJL*, 695, L35
- Gotthelf, E. V., Halpern, J. P., Alford, J. 2013a, *ApJ*, 765, 58
- Gotthelf, E. V., Halpern, J. P., Allen, B., & Knispel, B. 2013b, *ApJ*, 773, 141
- Gotthelf, E. V., Halpern, J. P., & Seward, F. D. 2005, *ApJ*, 627, 390
- Halpern, J. P., Bogdanov, S. & Gotthelf, E. V. 2013, *ApJ*, 778, 120
- Halpern, J. P., & Gotthelf, E. V. 2010, *ApJ*, 709, 436
- Halpern, J. P., & Gotthelf, E. V. 2011, *ApJL*, 736, L3
- Halpern, J. P., & Gotthelf, E. V. 2015, *ApJ*, 812, 61
- Halpern, J. P., Gotthelf, E. V., Camilo, F., & Seward, F. D. 2007, *ApJ*, 665, 1304
- Ho, W. C. G. 2011, *MNRAS*, 414, 2567
- Ho, W. C. G. 2015, *MNRAS*, 452, 845
- Kaspi, V. M., Gavriil, F. P., Woods, P. M., et al. 2003, *ApJL*, 588, L93
- Keane, E. F. & Kramer, M. 2008, *MNRAS*, 391, 2009
- Link, B., Franco, L. M., & Epstein, R. I. 1998, *ApJ*, 508, 838
- Lyne, A. G., Stappers, B. W., Freire, P. C. C., et al. 2017, *ApJ*, 834, 72
- Luo, J., Ng, C.-Y., Ho, W. C. G., et al. 2015, *ApJ*, 808, 130
- Macy, W. W., Jr. 1974, *ApJ*, 190, 153
- Menou, K., Esin, A., Narayan, R., et al. 1999, *ApJ*, 520, 276
- Mereghetti, S., De Luca, A., Caraveo, P. A., et al. 2002, *ApJ*, 581, 1290
- Pérez-Azorín, J. F., Miralles, J. A., & Pons, J. A. 2006, *A&A*, 451, 1009
- Pons, J. A., Miralles, J. A., & Geppert, U. 2009, *A&A*, 496, 207
- Sanwal, D., Pavlov, G. G., Zavlin, V. E., & Teter, M. A. 2002, *ApJ*, 574, 61
- Shabaltas, N. & Lai, D. 2012, *ApJ*, 748, 148
- Strüder, L., Briel, U., Dennerl, K., et al. 2001, *A&A*, 365, L18
- Suleimanov, V. E., Pavlov, G. G., & Werner, K. 2010, *ApJ*, 714, 635
- Thompson, C., & Duncan, R. C. 1993, *ApJ*, 408, 194
- Turner, M. J. L., Abbey, A., Arnaud, M., et al. 2001, *A&A*, 365, L27
- Verner, D. A., Ferland, G. J., Korista, K. T., Yakovlev, D. G. 1996, *ApJ*, 465, 487
- Viganò, D. & Pons, J. A. 2012, *MNRAS*, 425, 2487
- Wilms, J., Allen, A., & McCray, R. 2000, *ApJ*, 542, 914
- Zavlin, V. E., Pavlov, G. G., Sanwal, D., & Trümper 2000, *ApJ*, 540, L25